

Intrinsic vs. extrinsic anomalous Hall effect in ferromagnets

Shigeki Onoda,¹ Naoyuki Sugimoto,² and Naoto Nagaosa^{2,3}

¹ Spin Superstructure Project, ERATO, Japan Science and Technology Agency, c/o Department of Applied Physics, University of Tokyo, Tokyo 113-8656, Japan

² CREST, Department of Applied Physics, University of Tokyo, Tokyo 113-8656, Japan

³ Correlated Electron Research Center, National Institute of Advanced Industrial Science and Technology, Tsukuba, Ibaraki 305-8562, Japan

(dated: March 23, 2022)

A unified theory of the anomalous Hall effect (AHE) is presented for multi-band ferromagnetic metallic systems with dilute impurities. In the clean limit, the AHE is mostly due to the extrinsic skew-scattering. When the Fermi level is located around anti-crossing of band dispersions split by spin-orbit interaction, the intrinsic AHE to be calculated *ab initio* is resonantly enhanced by its non-perturbative nature, revealing the extrinsic-to-intrinsic crossover which occurs when the relaxation rate is comparable to the spin-orbit interaction energy.

PACS numbers: 72.15.Eb, 72.15.Lh, 72.20.My, 75.47.-m

Early experimental works on the Hall effect in ferromagnetic metals led a semi-empirical relation of the Hall resistivity ρ_{xy} to a weak applied magnetic field H and the spontaneous magnetization M both along the z direction; $\rho_{xy} = R_H H + 4 R_S M$ with the normal and the anomalous Hall coefficients R_H and R_S , respectively [1]. This anomalous Hall effect (AHE) [1] has been one of the most fundamental and intriguing but controversial issues in condensed-matter physics [2, 3, 4, 5, 6, 7]. It has not been clarified yet if the AHE is originated purely from extrinsic scattering or has an intrinsic contribution from the electronic band structure, which penetrates even recent debates on the interpretation of the experiments [8, 9, 10]. Theoretically, a unified description of both intrinsic and extrinsic contributions is called for but has not been considered seriously. It even reveals their nontrivial interplay and crossover and explains the AHE in a whole region from the clean limit to the hopping-conduction region (see Fig. 4), which are main goals of the present study.

Dissipationless and topological nature of the Hall effect has been highlighted by the discovery of the quantum Hall effect [1] in two-dimensional electron systems under a strong magnetic field. In the Streda formula [2] of the electric conductivity tensor $\rho_{ij}^{\text{tot}} = \rho_{ij}^{\text{I}} + \rho_{ij}^{\text{II}}$, in ideal cases where the Fermi level is located within the energy gap, the Fermi-surface contribution ρ_{ij}^{I} vanishes and the quantum contribution ρ_{ij}^{II} yields the TKNN formula [3]

$$\rho_{ij}^{\text{TKNN}} = \frac{e^2}{2\pi} \sum_n \int_{\text{BZ}} \frac{d^d p}{(2\pi)^d} b_n^z(\mathbf{p}) f'(\epsilon_n(\mathbf{p})) \quad (1)$$

with the electronic charge e , the Planck constant $\hbar = 2\pi$, the Fermi distribution function $f(\epsilon)$, and the antisymmetric tensor ρ_{ij}^{I} . We have introduced the eigenenergy $\epsilon_n(\mathbf{p})$, the Berry curvature $b_n^z(\mathbf{p}) = \mathbf{r}_p \cdot \mathbf{a}_n(\mathbf{p})$ and the Berry connection $\mathbf{a}_n(\mathbf{p}) = i\hbar \langle \mathbf{j}_p | \nabla_{\mathbf{p}} | \mathbf{j}_p \rangle$ of the generalized Bloch wave function $|\mathbf{j}_p\rangle$ with the band index n

and the Bloch momentum \mathbf{p} . Each band has a topological integer called the Chern number $C_n = \frac{1}{2\pi} \int_{\text{BZ}} \frac{d^d p}{(2\pi)^d} b_n^z(\mathbf{p})$. Their summation over the occupied bands determines the integer (Chern number) for the quantization $\rho_{xy}^{\text{tot}} = e^2 \hbar$ in insulators. Then, adiabatic semi-classical wave-packet equations have been devised to incorporate this Berry-curvature effect into the equations of motion [4].

Historically, Klapush-Luttinger [2] initiated an intrinsic mechanism of the AHE in a band model for ferromagnetic metals with the spin-orbit interaction, which coincides with the TKNN formula ρ_{xy}^{TKNN} [15, 16]. This reflects that the spin-orbit interaction bears a nontrivial topological structure in the Bloch wave functions of ferromagnets by splitting band dispersions, which originally cross at a certain momentum \mathbf{p}_0 , with a transfer of Chern numbers among the bands. This phenomenon called "parity anomaly" has a non-perturbative nature [17], and points to an importance of the anti-crossing points with a small gap $2\epsilon_0$, which is identified with the spin-orbit interaction energy ϵ_{SO} . When the Fermi level is located around such anti-crossing of dispersions, as found in recent *ab initio* calculations for SrRuO_3 [18] and the bcc Fe [19], the magnitude of ρ_{xy}^{TKNN} is resonantly enhanced and approaches $e^2 \hbar = 3.87 \times 10^5 \text{ } \Omega^{-1}$ in two dimensions and $e^2 \hbar a^{-1} \text{ cm}^{-1}$ in three dimensions with the lattice constant $a \approx 4 \text{ \AA}$ [18, 19].

On the other hand, adiabatic semi-classical Boltzmann transport analyses suggest that impurity scattering produces the AHE through the "skewness" [3, 5, 7] or the side jump [4, 7]. The skew-scattering contribution diverges in the clean limit as $\rho_{xy}^{\text{skew}} = \rho_{xx} S = \frac{2e^2}{\hbar a} \frac{E_F}{\epsilon_0} S$ with the lifetime τ and the Fermi energy E_F . Here, $S = \epsilon_{\text{SO}} v_{\text{imp}} / W^2$ (1) is the skewness factor with W being the bandwidth or the inverse of the density of states and v_{imp} the impurity potential strength.

Generic model that fully takes into account both the "parity anomaly" associated with the anti-crossing of band dispersions and the impurity scattering can be ob-

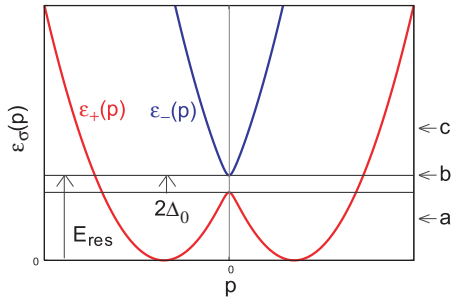


FIG. 1: (Color online) Energy dispersions for the Hamiltonian \hat{H}_0 in Eq. (2).

tained by expanding the Hamiltonian at a fixed p_z with respect to the momentum p measured from the originally crossing point p_0 of two dispersions;

$$\hat{H}_0 + \hat{H}_{\text{imp}} = \epsilon_0^2 + v p \hat{e}_z^2 + \frac{p^2}{2m} + v_{\text{imp}} \sum_{\mathbf{r}_{\text{imp}}} \chi(\mathbf{r}_{\text{imp}}) \quad (2)$$

with the position \mathbf{r} of electron, the Pauli matrices $\hat{\alpha} = (\hat{\alpha}_x; \hat{\alpha}_y; \hat{\alpha}_z)$, the unit vector \hat{e}_z in the z direction, and an impurity at a position \mathbf{r}_{imp} . The first term corresponds to the level splitting $2\epsilon_0 = \epsilon_{S_0}$ of two bands at the anti-crossing momentum. The second term gives the linear dispersion with the velocity v . The third term represents the quadratic dispersion with an effective mass m , whose anisotropy has been neglected since it is unimportant. This model has two band dispersions $\epsilon_{\pm}(p)$ as shown in Fig. 1. Henceforth, the bottom of the lower band is chosen as the origin of the energy and the bottom of the upper band denoted as $E_{\text{res}} = \epsilon_0(0)$ is taken as an energy unit. The model possesses the gauge flux $\mathcal{B}_{\text{imp}} = \frac{2\epsilon_0}{p}$ with $p = \sqrt{2p^2 + \frac{2}{\epsilon_0}}$ [20, 21]. In the case of resonance, $E_F \approx [E_{\text{res}} - 2\epsilon_0; E_{\text{res}}]$, χ_{xy}^{TKNN} approaches the maximum value $e^2 = 2h$. Away from this resonance, dominant contributions from the momentum region around $p = 0$ cancel out each other or do not appear, leading to a suppression of χ_{xy}^{TKNN} ($\epsilon^2 = h$) ($\epsilon_{S_0} = E_F$), where the perturbation expansion in ϵ_{S_0} is justified. Therefore, the present model, Eq. (2), can be regarded as a generic continuum model for a momentum region that gives a major contribution to the AHE. By definition of the anti-crossing, ϵ_0 does not change its sign as a function of p_z . This removes a concern that the integration over p_z might lead to a cancellation.

We employ the Keldysh formalism for non-equilibrium Green's functions, which has recently been reformulated for generic multi-component systems [22]. We consider Green's functions and self-energies under an applied constant electric field $E = (0; E_y)$; $\hat{G}^{\text{R/A}}(\omega; p)$ and $\hat{\Sigma}^{\text{R/A}}(\omega)$ with $\omega = R; A; <$ for the retarded, advanced and lesser components, respectively. ω and p represent the covariant energy and momentum in the Wigner representation [22].

$\hat{G}^{\text{R/A}}(\omega; p)$ and $\hat{\Sigma}^{\text{R/A}}(\omega)$ can be expanded in E_y as

$$\hat{G}^{\text{R/A}}(\omega; p) = \hat{G}_0^{\text{R/A}}(\omega; p) + e E_y \hat{G}_{E_y}^{\text{R/A}}(\omega; p) + O(E_y^2); \quad (3)$$

$$\hat{\Sigma}^{\text{R/A}}(\omega) = \hat{\Sigma}_0^{\text{R/A}}(\omega) + e E_y \hat{\Sigma}_{E_y}^{\text{R/A}}(\omega) + O(E_y^2); \quad (4)$$

Henceforth, functionals with the subscripts 0 and E_y denote those in the absence of and the gauge-invariant linear response to E_y . Due to the ω -functional form of the impurity potential, the self-energies are local. $\hat{G}_0^{\text{R/A}}$ satisfies the familiar Dyson equation,

$$\hat{G}_0^{\text{R/A}}(\omega; p) = [\omega - \hat{H}_0(p) - \hat{\Sigma}_0^{\text{R/A}}(\omega)]^{-1}; \quad (5)$$

The self-consistent equations for $\hat{G}_{E_y}^{\text{R/A}; <}$ are obtained by expanding the Dyson equation in the electric field [2]. It is convenient to decompose $\hat{G}_{E_y}^{\text{R/A}; <}$ and $\hat{\Sigma}_{E_y}^{\text{R/A}; <}$ into two;

$$\hat{G}_{E_y}^{\text{R/A}; <}(\omega; p) = \hat{G}_{E_y; I}^{\text{R/A}; <}(\omega; p) f(\omega) + \hat{G}_{E_y; II}^{\text{R/A}; <}(\omega; p) f(\omega) \quad (6)$$

$$\hat{\Sigma}_{E_y}^{\text{R/A}; <}(\omega) = \hat{\Sigma}_{E_y; I}^{\text{R/A}; <}(\omega) f(\omega) + \hat{\Sigma}_{E_y; II}^{\text{R/A}; <}(\omega) f(\omega) \quad (7)$$

$$\hat{G}_{E_y; I}^{\text{R/A}; <}(\omega; p) = \hat{G}_{E_y}^{\text{R/A}}(\omega; p) - \hat{G}_{E_y}^{\text{R/A}}(\omega; p) \quad (8)$$

$$\hat{\Sigma}_{E_y; I}^{\text{R/A}; <}(\omega) = \hat{\Sigma}_{E_y}^{\text{R/A}}(\omega) - \hat{\Sigma}_{E_y}^{\text{R/A}}(\omega); \quad (9)$$

$\hat{G}_{E_y; I}^{\text{R/A}; <}$ and $\hat{\Sigma}_{E_y; I}^{\text{R/A}; <}$ can be self-consistently determined from the quantum Boltzmann equation in the first order in E_y ,

$$\begin{aligned} & \hat{G}_{E_y; I}^{\text{R/A}; <}(\omega; p) \hat{H}_0 + \hat{G}_{E_y; I}^{\text{R/A}; <}(\omega; p) \hat{\Sigma}_0^{\text{R/A}} + \hat{G}_0^{\text{R/A}} \hat{G}_{E_y; I}^{\text{R/A}; <}(\omega; p) \\ & = \hat{\Sigma}_{E_y; I}^{\text{R/A}; <}(\omega) \hat{G}_0^{\text{R/A}} + \hat{G}_0^{\text{R/A}} \hat{\Sigma}_{E_y; I}^{\text{R/A}; <}(\omega) + \frac{i}{2} \hat{\mathcal{V}}_y \hat{G}_0^{\text{R/A}} + \hat{G}_0^{\text{R/A}} \hat{\mathcal{V}}_y \\ & + \frac{i}{2} (\hat{\mathcal{V}}_0^{\text{R/A}} - \hat{\mathcal{V}}_0^{\text{R/A}}) (\hat{\mathcal{G}}_0^{\text{R/A}}) + (\hat{\mathcal{G}}_0^{\text{R/A}}) (\hat{\mathcal{V}}_0^{\text{R/A}} - \hat{\mathcal{V}}_0^{\text{R/A}}) \end{aligned} \quad (10)$$

with the velocity $\hat{\mathcal{V}}_i(p) = \partial_{p_i} \hat{H}_0(p)$, while $\hat{G}_{E_y}^{\text{R/A}}$ and $\hat{\Sigma}_{E_y}^{\text{R/A}}$ are determined from the other self-consistent equation,

$$\begin{aligned} \hat{G}_{E_y}^{\text{R/A}} & = \hat{G}_0^{\text{R/A}} \hat{\Sigma}_{E_y}^{\text{R/A}} \hat{G}_0^{\text{R/A}} \\ & + \frac{i}{2} \hat{G}_0^{\text{R/A}} \hat{\mathcal{V}}_y (\hat{\mathcal{G}}_0^{\text{R/A}}) + (\hat{\mathcal{G}}_0^{\text{R/A}}) \hat{\mathcal{V}}_y \hat{G}_0^{\text{R/A}}; \end{aligned} \quad (11)$$

We can exactly calculate the self-energies $\hat{\Sigma}_0^{\text{R/A}}$ and $\hat{\Sigma}_{E_y}^{\text{R/A}; <}$ up to the n_{imp} -linear terms by means of the T-matrix approximation;

$$\hat{\Sigma}_0^{\text{R/A}}(\omega) = n_{\text{imp}} \hat{T}_0^{\text{R/A}}(\omega) \quad (12)$$

$$\hat{T}_0^{\text{R/A}}(\omega) = v_{\text{imp}}^{-1} \sum_{\mathbf{p}} \frac{d^2 p}{(2\pi)^2} \hat{G}_0^{\text{R/A}}(\omega; p) \quad (13)$$

for the zeroth-order in E_y and

$$\hat{\Sigma}_{E_y; I}^{\text{R/A}; <}(\omega) = n_{\text{imp}} \hat{T}_0^{\text{R/A}}(\omega) \sum_{\mathbf{p}} \frac{d^2 p}{(2\pi)^2} \hat{G}_{E_y; I}^{\text{R/A}; <}(\omega; p) \hat{T}_0^{\text{R/A}}(\omega) \quad (14)$$

$$\hat{\Sigma}_{E_y}^{\text{R/A}}(\omega) = n_{\text{imp}} \hat{T}_0^{\text{R/A}}(\omega) \sum_{\mathbf{p}} \frac{d^2 p}{(2\pi)^2} \hat{G}_{E_y}^{\text{R/A}}(\omega; p) \hat{T}_0^{\text{R/A}}(\omega) \quad (15)$$

for the first-order in E_y . We solve Eqs. (5), (12) and (13) self-consistently to obtain $\hat{G}_0^{\text{R/A}}$ and $\hat{\Sigma}_0^{\text{R/A}}$. Next, they

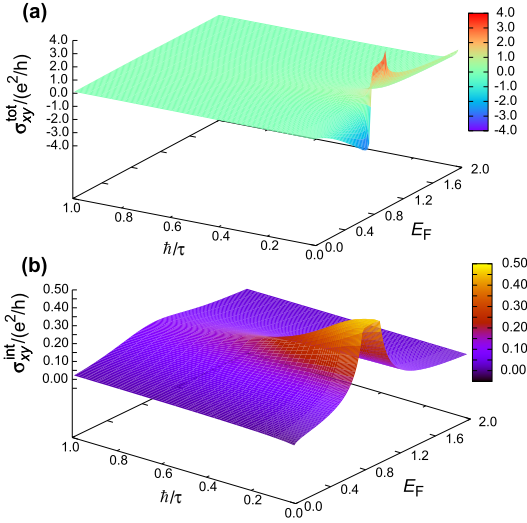


FIG. 2: (Color) (a) The total anomalous Hall conductivity σ_{xy}^{tot} against E_F and \sim in an energy unit of $E_{\text{res}} = 1.0$. (b) The intrinsic contribution σ_{xy}^{int} for the same parameter values. Note the difference of the scales for σ_{xy} in (a) and (b).

are plugged into Eqs. (10) and (14) to solve $\hat{G}_{E_y;I}^<$ and $\hat{G}_{E_y;I}^<$ self-consistently. $\hat{G}_{E_y}^R;A$ and $\hat{G}_{E_y}^R;A$ are obtained from Eqs. (11) and (15), and hence $\hat{G}_{E_y;II}^<$ through Eq. (8). The conductivity tensors are calculated from

$$\begin{aligned} \sigma_{ij}^I &= \frac{e^2 \sim}{2i} \frac{\int d^2p}{(2\sim)^2} \text{Tr} \hat{v}_i(p) \hat{G}_{E_j;I}^<(\sim;p); \\ \sigma_{ij}^{II} &= e^2 \sim \frac{\int d^2p}{(2\sim)^2} \text{Tr} \hat{v}_i(p) \hat{G}_{E_j;II}^<(\sim;p) f(\sim). \end{aligned} \quad (16)$$

with $i,j = x,y$. Note that Eqs. (16) and (17) are along the same spirit as the Streda formula [2]: this approach provides the diagrammatic treatment for the Streda formula [22]. Effects of the vertex corrections to $\hat{G}_{E_j;II}^<$ cancel each other, and hence we can regard σ_{xy}^{II} as an intrinsic contribution. By contrast, the Fermi-surface contribution σ_{xy}^I suffers from a vertex correction. While the intra-band matrix elements correspond to the conventional description of both σ_{xx} and σ_{xy} based on the scattering events, the inter-band ones contain a finite intrinsic contribution to the AHE as a part of the Berry-curvature term [23] and is generically expressed as

$$\begin{aligned} \sigma_{ij}^{\text{int}} &= \frac{e^2 \sim}{2} \frac{\int dp}{(2\sim)^d} \sum_{n,m^0} \text{Re} \left[\langle n | \hat{v}_j | m^0 \rangle \langle m^0 | \hat{v}_i | n \rangle \right]; \end{aligned} \quad (18)$$

Figure 2(a) shows the numerical results on $\sigma_{xy}^{\text{tot}} = \sigma_{xy}^I + \sigma_{xy}^{II}$ against the Fermi energy E_F and the Born scattering amplitude $\sim = \frac{1}{n_{\text{imp}} v_{\text{imp}}^2 m}$ for a typical set of parameters, $\mu_0 = 0.1$, $2m v_{\text{imp}} = 0.6$, $2m^2 = 3.59$,

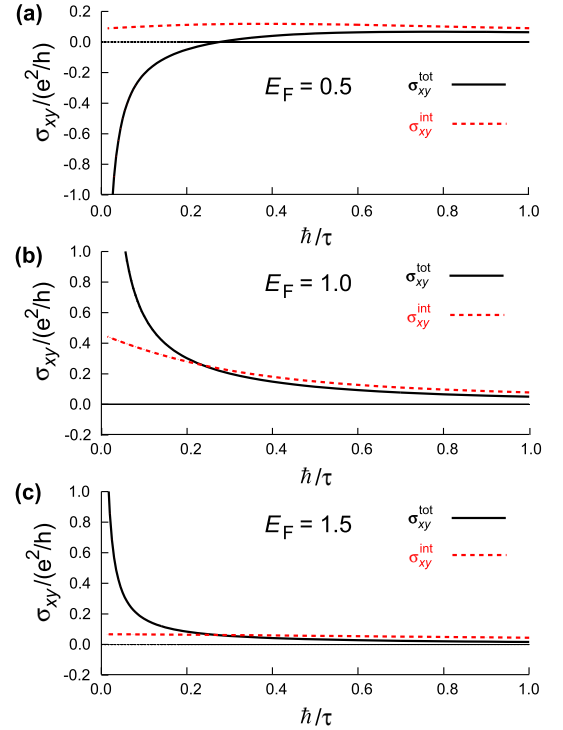


FIG. 3: (Color online) σ_{xy}^{tot} and σ_{xy}^{int} as a function of \sim for the same parameter values as Fig. 2 with $E_F = 0.5, 1.0$ and 1.5 for (a), (b), and (c), respectively.

and the energy cutoff is taken as $E_c = 3.0$ in an energy unit of $E_{\text{res}} = 1.0$ [24]. In the clean limit $\sim \rightarrow 0$, σ_{xy}^{tot} diverges in accordance with the skew-scattering scenario. Strength of the divergence is proportional to E_F in the low electron-density limit, and the sign is inverted around $E_F = \mu_0 = E_{\text{res}}/2$. Sign of the skew-scattering contribution also changes by the sign change of v_{imp} . Figure 2(b) shows the intrinsic contribution σ_{xy}^{int} calculated by imposing $\hat{G}_{E_y}^R;A;E = 0$ for the same set of parameters. Under the resonant condition for E_F , σ_{xy}^{int} becomes of the order of $e^2/2h$. With increasing \sim , it gradually decreases solely due to damping of quasi-particles.

By contrast, with increasing \sim , the extrinsic skew-scattering contribution rapidly decays (Fig. 3), reflecting that it originates purely from intra-band processes and hence the skewness factor S remains of the order of $\mu_{S0} v_{\text{imp}} = W^2$. In moderately dirty cases, the total conductivity nearly merges into the intrinsic value. Namely, there appears a crossover from the extrinsic regime to the intrinsic as \sim increases. Especially in the resonant case ($E_F = E_{\text{res}}$) shown in Fig. 3(b), the intrinsic contribution is significantly enhanced and the extrinsic-to-intrinsic crossover occurs at $\sim = \mu_{S0}$. For a small ratio of $\mu_{S0} = E_F/10^3 - 10^2$ [18, 19], dominance of the intrinsic AHE is realized within the usual clean metal. In reality, the total Hall conductivity is the sum of the con-

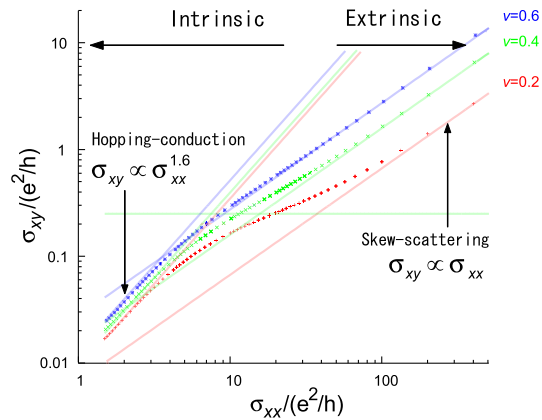


FIG. 4: (Color online) Scaling plot of σ_{xy} versus σ_{xx} for the same sets of parameter values as in Fig. 3 (b) except for $2m v_{\text{imp}}$.

contributions from all over the Brillouin zone. Since skew-scattering contributions from other momentum regions are always subject to a similar rapid decay, the above extrinsic-to-intrinsic crossover still occurs unless contributions from all the anti-crossing regions of band dispersions are mutually canceled out by accident.

Figure 4 shows the logarithmic plot of σ_{xy} against σ_{xx} for the same set of parameters as Fig. 3 (b) except for the impurity scattering strength v_{imp} , which is varied for different curves. In the clean limit, the curves nicely follow $\sigma_{xy} / \sigma_{xx}$ and the ratio $\sigma_{xy} / \sigma_{xx}$ is proportional to v_{imp} for a fixed $\sigma_{xx} = 2(e^2/h)E_F = \tilde{\omega}$ decreases with decrease in $\tilde{\omega}$, the relation exhibits an upward deviation from the linear one, signalling the crossover to the intrinsic regime. A smaller impurity potential strength v_{imp} enlarges the region of the constant behaviour of σ_{xy} . (Note that we change v_{imp} to control $\tilde{\omega}$.) Careful experiments are required to test the prediction of the crossover at low temperatures. The magnitude of σ_{xy} in the intrinsic regime is consistent with experimentally observed values $\sigma_{xy} = 10^2 - 10^3 \text{ cm}^{-1}$ in a σ_{xy} -constant region of Fe- and Ni-based dilute alloys [1], and SrRuO_3 and metallic foils [25]. Further decrease of $\tilde{\omega}$ again changes the scaling behaviour to $\sigma_{xy} / \sigma_{xx}^{1.6}$, which almost agrees with recent experiments on a disordered pyrochlore ferromagnet $\text{Nd}_2(\text{Mo}_{1-x}\text{Nb}_x)_2\text{O}_7$ [26] and on $\text{La}_{1-x}\text{Sr}_x\text{CoO}_3$ [25]. This exponent approximates to the value expected for the normal Hall effect in the hopping conduction regime [27].

Now the source of the confusion over decades is clear. The skew-scattering contribution, though it is rather sensitive to details of the impurity potential and band structure, can be larger than e^2/h in the superclean case $\tilde{\omega} = \omega_{s_0}$, but decays for $\omega_{s_0} < \tilde{\omega}$. The side-jump contribution is smaller and of the order of $(e^2/h)(\omega_{s_0} = E_F)$ [7]. Therefore, the intrinsic one, which is of the order of e^2/h under the resonant condition, is dominant over a wide range of the scattering strength

$\omega_{s_0} < \tilde{\omega} < E_F$ (clean case). Although Luttinger reconsidered the Karplus-Luttinger theory [2] and gave an expansion of σ_{xy} in v_{imp} , including the skew-scattering contribution as well [5], it fails to reveal the above crossover in the space of E_F , ω_{s_0} and $\tilde{\omega}$.

In conclusion, we have shown that the AHE is determined by the intrinsic mechanism when (i) the Fermi level is located around an anti-crossing of band dispersions in the momentum space, (ii) consequently the magnitude of σ_{xy} is comparable to e^2/h ($\approx 10^3 \text{ cm}^{-1}$), and (iii) the resistivity ρ_{xx} is larger than (h/e^2) ($\omega_{s_0} = E_F$) $1-10 \text{ cm} \cdot \text{W}$. With these conditions, first-principle calculation can give an accurate prediction of σ_{xy} . The present work resolves a long standing controversy on the mechanism of the AHE in a whole region.

The authors are grateful to A. A. Samitsu, T. Miyazato, S. Iguchi, R. Mathieu, and Y. Tokura for fruitful discussion and showing unpublished experimental data, and H. Fukuyama, A. H. MacDonald, J. Sinova, J. Inoue, S. Murakami, K. Nomura, and M. Onda for stimulating discussion. Numerics was performed using the supercomputer at the Institute of Solid State Physics, University of Tokyo. The work was supported by Grant-in-Aids and NAREGINanoscience Project from the Ministry of Education, Culture, Sports, Science, and Technology.

Electronic address: sonoda@appit.u-tokyo.ac.jp

- [1] C. M. Hurd, *The Hall Effect in Metals and Alloys* (Plenum Press, New York, 1972).
- [2] R. Karplus and J. M. Luttinger, *Phys. Rev.* **95**, 1154 (1954).
- [3] J. Smith, *Physica* **21**, 877 (1955).
- [4] L. Berger, *Phys. Rev. B* **2**, 4559 (1970).
- [5] J. M. Luttinger, *Phys. Rev.* **112**, 739 (1958).
- [6] J. Kondo, *Prog. Theor. Phys.* **27**, 772 (1962).
- [7] P. Nozières and C. Lewiner, *J. Phys. (Paris)* **34**, 901 (1973).
- [8] H. Ohno, *Science* **281**, 951-956 (1998).
- [9] W.-L. Lee et al., *Science* **303**, 1647 (2004).
- [10] N. M. Anyala et al., *Nature Materials* **3**, 255 (2004).
- [11] R. E. Prange and S. M. Girvin, (eds.) *The Quantum Hall Effect* (Springer, Berlin, 1987).
- [12] P. Streda, *J. Phys. C: Solid State Phys.* **15**, L717 (1982).
- [13] D. J. Thouless et al., *Phys. Rev. Lett.* **49**, 405 (1982).
- [14] G. Sundaram and Q. Niu, *Phys. Rev. B* **59**, 14915 (1999).
- [15] M. Onda and N. Nagaosa, *J. Phys. Soc. Jpn.* **71**, 19 (2002).
- [16] T. Jungwirth, Q. Niu, and A. H. MacDonald, *Phys. Rev. Lett.* **88**, 207208 (2002).
- [17] R. Jackiw, *Phys. Rev. D* **29**, 2375 (1984).
- [18] Z. Fang et al., *Science* **302**, 92 (2003).
- [19] Y. Yao et al., *Phys. Rev. Lett.* **92**, 037204 (2004).
- [20] V. K. Dugaev et al., *Phys. Rev. B* **71**, 224423 (2005).
- [21] N. A. Sinitsyn et al., *Phys. Rev. B* **72**, 045346 (2005).
- [22] S. Onda, N. Sugimoto, and N. Nagaosa, *Prog. Theor. Phys.* **116**, 61 (2006), and references therein.
- [23] N. A. Sinitsyn et al., *cond-mat/0602598*.

- [24] Non-scalar relaxation rate leads to $\chi_{xy} \neq 0$ even for $E_F > E_{\text{res}}$ [J. Inoue et al, cond-mat/0604108].
- [25] T. Miyazato et al, private communication.
- [26] S. Iguchi et al, private communication.
- [27] L. P. Pryadko and A. Auerbach, Phys. Rev. Lett. 82, 1253 (2004).